Semiconductor–Insulator–Semiconductor Diode Consisting of Monolayer MoS_2, h-BN, and GaN Heterostructure

Hyun Jeong,[†,‡] Seungho Bang,[†,∥] Hye Min Oh,[†,∥] Hyeon Jun Jeong,[†,∥] Sung-Jin An,[†,∥] Gang Hee Han,[†] Hyun Kim,[†,∥] Ki Kang Kim,[§] Jin Cheol Park,[†,∥] Young Hee Lee,[†,∥] Gilles Lerondel,[‡,∥] and Mun Seok Jeong*[,†,∥]

[†]Center for Integrated Nanostructure Physics, Institute for Basic Science, Sungkyunkwan University, Suwon 440-746, Republic of Korea, [‡]Laboratoire de Nanotechnologie et d'Instrumentation Optique, Institut Charles Delaunay, CNRS-UMR 6281, Université de Technologie de Troyes, BP 2060, 10010 Troyes, France, [§]Department of Energy and Materials Engineering, Dongguk University, Seoul 100-715, Republic of Korea, and [∥]Department of Energy Science, Sungkyunkwan University, Suwon 440-746, Republic of Korea

ABSTRACT

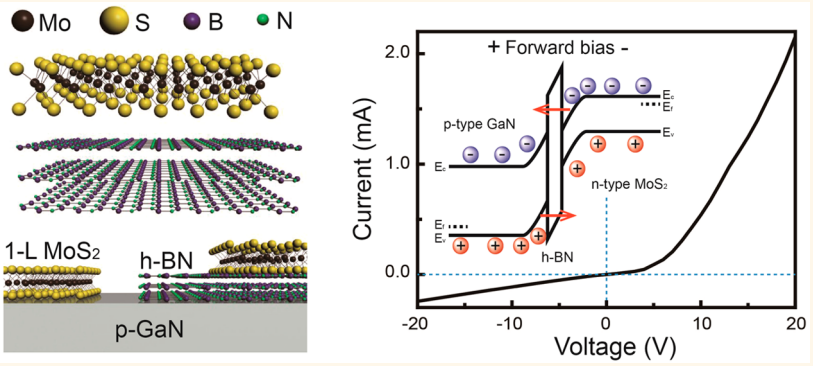

We propose a semiconductor–insulator–semiconductor (SIS) heterojunction diode consisting of monolayer (1-L) MoS_2, hexagonal boron nitride (h-BN), and epitaxial p-GaN that can be applied to high-performance nanoscale optoelectronics. The layered materials of 1-L MoS_2 and h-BN, grown by chemical vapor deposition, were vertically stacked by a wet-transfer method on a p-GaN layer. The final structure was verified by confocal photoluminescence and Raman spectroscopy. Current–voltage (*I*–*V*) measurements were conducted to compare the device performance with that of a more classical p–n structure. In both structures (the p–n and SIS heterojunction diode), clear current-rectifying characteristics were observed. In particular, a current and threshold voltage were obtained for the SIS structure that was higher compared to that of the p–n structure. This indicated that tunneling is the predominant carrier transport mechanism. In addition, the photoresponse of the SIS structure induced by the illumination of visible light was observed by photocurrent measurements.

KEYWORDS: monolayer MoS_2 · h-BN · GaN · semiconductor–insulator–semiconductor diode · carrier tunneling

In recent years, significant progress has been made in the application of two-dimensional (2D) layered materials having individual planes with an atomic-scale thickness.[1−4] In particular, 2D transition-metal dichalcogenides (TMDs) have emerged as significant 2D layered materials for applications in nanoscale electronics and optoelectronics.[5−8] As a representative TMD material, monolayer (1-L) MoS_2 with a direct optical transition band of 1.8 eV has been widely researched because of its strong photoluminescence (PL) and high photoresponsivity at room temperature.[9−12] Because of the peculiar characteristics of TMD materials, such as a high transparency, good flexibility, an atomically thin structure, and predictable electron transport, vertically stacked 2D layered materials have recently attracted much attention.[13−15] In particular, a heterojunction diode consisting of layered materials is emerging as a prospective device for next-generation nanoscale electronics.[16−18]

* Address correspondence to mjeong@skku.edu.

Received for review June 14, 2015 and accepted October 4, 2015.

Published online October 04, 2015
10.1021/acsnano.5b04233

In typical diodes, the semiconductor−insulator−semiconductor (SIS) diode has considerable advantages compared to conventional p−n junction diodes. These advantages include the lack of a depletion region and a high current flow as a result of carrier tunneling.[19−23] Therefore, an SIS diode has a lower offset current under certain biases and a higher current flow above the threshold voltage than a p−n junction diode.

Herein, we propose a heterostructure device: an SIS diode consisting of 1-L MoS_2, hexagonal boron nitride (h-BN), and GaN, where 1-L MoS_2 and GaN are used as the semiconducting materials. The use of 1-L MoS_2 is appropriate owing to its stable optical and electrical properties at room temperature.[24−26] Furthermore, GaN is a promising material and suitable in combination with 1-L MoS_2 in an SIS diode because it has a strong optical transition with an energy band gap of 3.4 eV and high photoresponsivity characteristics.[27−31] Lately, GaN-based heterostructures with layered materials have been investigated, including GaN−graphene for electrically tunable light emitters[32] and GaN−MoS_2 for visible-light photocatalysts.[33] As an insulating layered material, h-BN is used because of its great thermal and dielectric stability.[34,35] Since h-BN has an energy band gap of 5.2 eV, it exhibits a high transparency in the visible spectral range. By using confocal PL and Raman spectroscopy, the optical properties of the semiconducting layers and vertically well-stacked layered materials were verified. The performance of the SIS diode compared to that of the p−n junction diode was examined by plotting conventional current−voltage (*I*−*V*) curves.

RESULTS AND DISCUSSION

The fabrication processes for the SIS diode and p−n junction diode, which consist of GaN and layered materials, are depicted in Figure 1a,b. A p-type GaN (p-GaN) layer was grown by metal−organic chemical vapor deposition on a (0001) *c*-plane sapphire substrate. For the SIS heterostructure, multiple layers of h-BN grown by chemical vapor deposition (CVD) were transferred onto the p-GaN layer, as represented in Figure 1a. The transfer processes for all of the layered materials were conducted by a conventional wet transfer method; see Experimental Methods. The final thickness of the transferred h-BN was approximately 20 nm. The dimensions of transferred h-BN on the p-GaN substrate were 2 cm × 2 cm. The 1-L MoS_2 flakes grown by CVD were transferred to both of the h-BN/p-GaN and p-GaN regions to realize the SIS and p−n heterojunction diodes, as depicted in Figure 1b.

Finally, 1-L MoS_2/h-BN/p-GaN and 1-L MoS_2/p-GaN heterostructures, which correspond to the SIS and p−n junctions, were formed on the same p-GaN substrate, as shown in Figure 1c. The 1-L MoS_2 flakes for the SIS and p−n heterojunction diodes were transferred from the same batch of samples grown by CVD to compare the device performance for each heterojunction

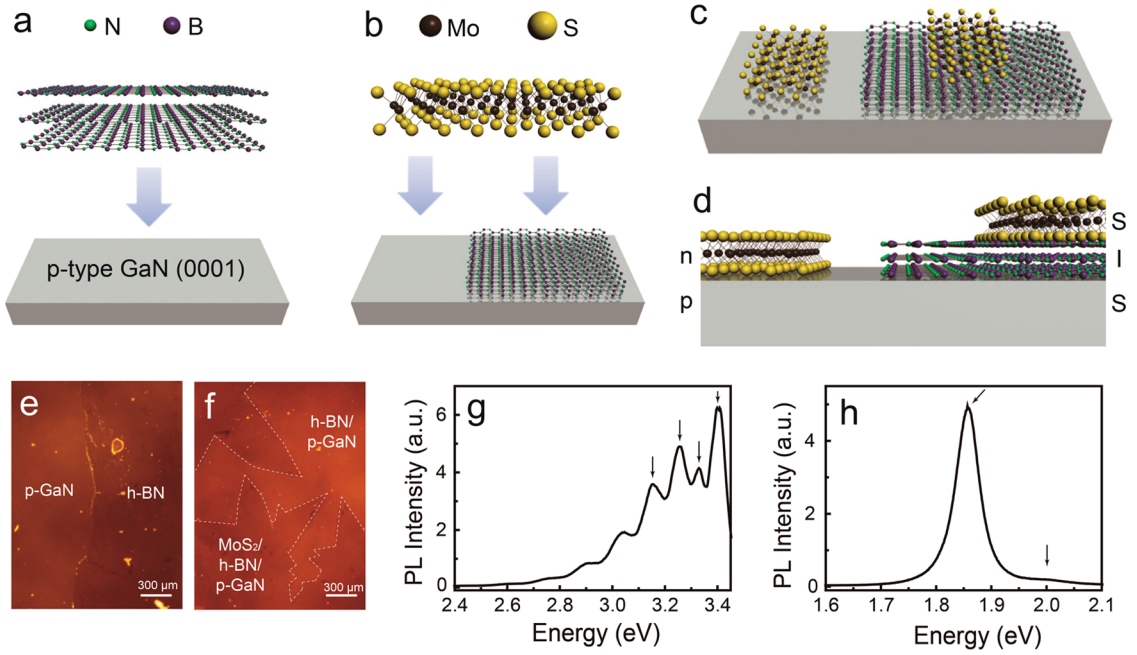

Figure 1. Schematics of the stacking process for (a) h-BN and (b) 1-L MoS_2. The 1-L MoS_2 and h-BN were sequentially stacked on an epitaxial p-GaN layer. (c) Perspective and (d) cross-sectional schematics of the final SIS and p−n heterojunction structures. To prevent leakage current, the size of the top layer is smaller than that of the layer underneath. Optical microscopy images show the (e) border of h-BN on p-GaN and (f) top surface including the edge of 1-L MoS_2 on h-BN/p-GaN. The SIS structure was vertically well-stacked with large MoS_2 flakes. Confocal PL spectra of the (g) p-GaN layer and (h) 1-L MoS_2.

structure under equivalent conditions. The dimensions of 1-L MoS_2 as an n-type semiconducting layer for both the SIS and p−n heterojunctions were 1.2 cm × 0.7 cm. Figure 1d shows a cross-sectional schematic of the final structure of the SIS and p−n heterojunction diodes. To make a reliable comparison between the SIS and p−n diodes, all of the layered materials are stacked on the same p-GaN substrate. Figure 1e,f shows optical microscope images for the boundary regions of h-BN/p-GaN and MoS_2 on h-BN/p-GaN, respectively. The white scale bar indicates 300 μm for both images. As shown in Figure 1e,f, a clear borderline for h-BN was observed in the expected area, which is realized by a controllable chemical transfer process of layered materials that allows for a specific stacking structure. The white dotted lines in Figure 1f indicate the border of the 1-L MoS_2 flakes. A 1-L MoS_2 flake is approximately 500 μm × 500 μm and has a linked triangular shape.

The local PL spectra of p-GaN and 1-L MoS_2 were measured by confocal PL spectroscopy, as shown in Figure 1g,h. The excitation source for the PL spectrum of p-GaN was a 355 nm diode-pumped solid-state (DPSS) laser. Spectroscopic measurements were completed at room temperature. Weak PL peaks were observed at 3.41, 3.32, 3.26, and 3.16 eV; these are marked with black arrows in Figure 1g. The PL peak at 3.41 eV corresponds to the free exciton transition of the GaN buffer layer, and the peak at 3.26 eV is induced by a shallow donor−acceptor pair (DAP) transition. The peaks at 3.32 and 3.16 eV are the phonon replicas of the peaks at 3.41 and 3.26 eV, respectively.[36] The strong DAP peak without a yellow band peak and the clearly observable phonon replicas support the conclusion that p-GaN has good p-type characteristics and a high crystalline quality. Figure 1h shows the PL spectrum of 1-L MoS_2, as observed by confocal microscopy using a 532 nm DPSS laser for excitation. As marked in the PL spectrum of 1-L MoS_2 with black arrows, the PL peaks of the A and B excitons of 1-L MoS_2 are observed at 1.85 and 2.02 eV, respectively.[37] In previous works, the PL peak for the A exciton of 1-L MoS_2 has been attributed to two contributions: the negative trion peak at 1.84 eV and the neutral exciton peak at 1.88 eV. The presence of the negative trion peak in the PL spectrum indicates that 1-L MoS_2 has electrically n-type characteristics.[38]

Confocal scanning Raman spectroscopy was employed for the spectroscopic verification of each vertically stacked material in the SIS heterostructure. A 532 nm DPSS laser was used as an excitation source for Raman spectroscopy. Figure 2a shows the confocal Raman image of a selected region that includes the border of the 1-L MoS_2. The bright area with a linked triangular shape is the fully overlapped region of MoS_2/h-BN/p-GaN. The relatively dark area is the h-BN/p-GaN region. The substantial Raman intensity fluctuation

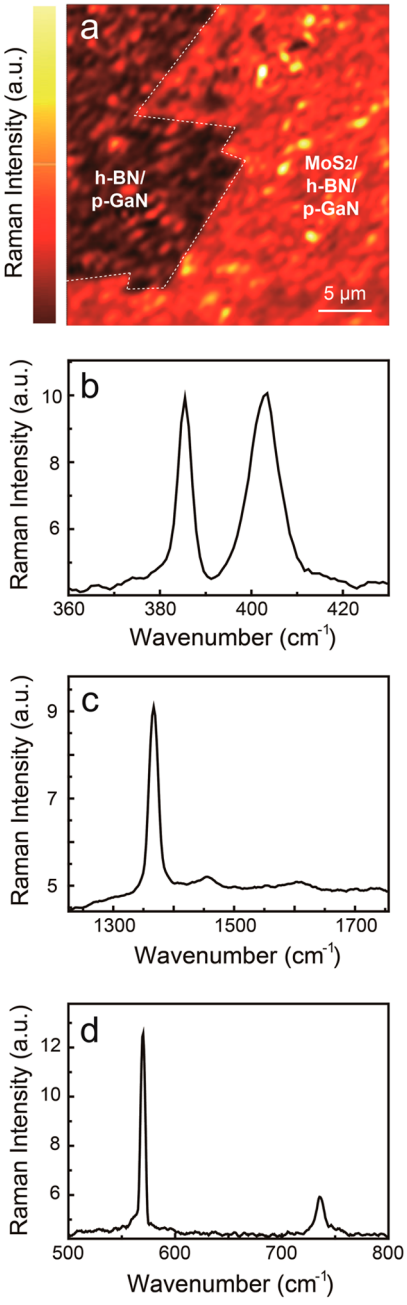

Figure 2. (a) Confocal Raman mapping image measured from the top surface of the SIS heterojunction structure. The brighter regions correspond to the fully stacked area of 1-L MoS_2/h-BN/p-GaN. Confocal Raman spectra for (b) 1-L MoS_2, (c) h-BN, and (d) p-GaN. Vertically well-stacked layered materials on the p-GaN were clearly observed through the confocal Raman results.

revealed in the confocal Raman image is attributed to the inhomogeneous crystalline quality of the p-GaN layer, as shown in Figure S1 of the Supporting Information. Figure 2b−d shows the Raman spectra for 1-L MoS_2, h-BN, and p-GaN, respectively. In the Raman spectrum of 1-L MoS_2, the E_{2g} and A_{1g} Raman modes are observed at 385 and 403 cm^{-1}, respectively, as shown in Figure 2b. The 18 cm^{-1} interval between these two peaks indicates that MoS_2 is a monolayer.[39] As can be seen in Figure 2c,

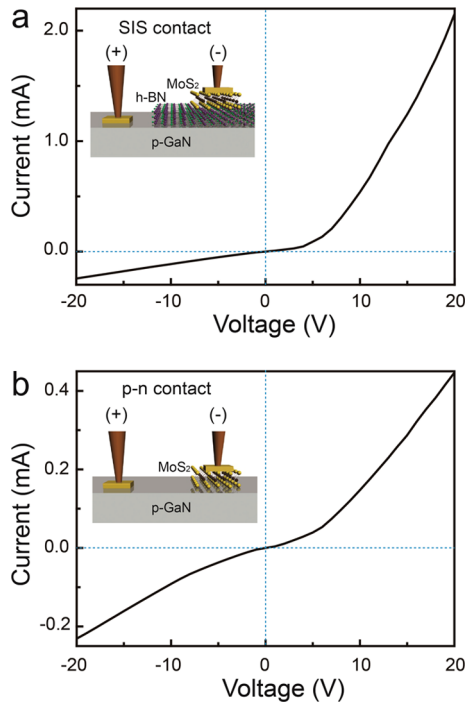

Figure 3. *I*–*V* curves of the (a) SIS and (b) p–n heterojunction structures. A higher threshold voltage with a much higher current was observed for the SIS structure compared to that with the p–n structure.

Raman scattering was observed at 1366 cm^{-1}, which corresponds to the E_{2g} mode of h-BN.[40] Figure 2d shows the E_2^{high} and A_1^{LO} modes for p-GaN at 570 and 735 cm^{-1}, respectively. These confocal Raman results imply that the layered materials are vertically stacked on p-GaN.

To evaluate the device performance of the SIS and p–n diodes consisting, respectively, of 1-L MoS_2, h-BN, and p-GaN and 1-L MoS_2 and p-GaN, *I*–*V* measurements were conducted. Gold-coated tungsten tips were used for the current injection and detection probes. As a robust electrode for the anode and cathode, Cr/Au was deposited onto p-GaN and 1-L MoS_2. The voltage range was from 0 to 20 V, and the distance between the metal tips was kept the same for both structures. This allowed a comparison of the *I*–*V* curves under equivalent conditions. The p-GaN and 1-L MoS_2 layers were used as an anode and a cathode, respectively, for both diode structures. Figure 3a shows the *I*–*V* curve for the SIS heterojunction diode. The inset shows a three-dimensional (3D) schematic of the configuration for the *I*–*V* measurements. A nonlinearly increasing current was observed above the threshold voltage range with a considerably low current at the milliampere scale, as shown in Figure 3a. The threshold voltage and series resistance of the SIS diode are approximately 5 V and 7.2×10^3 Ω, respectively. Figure 3b shows the *I*–*V* curve of the p–n heterojunction diode structure. The 3D schematic of the *I*–*V* configuration for the p–n diode is shown in the inset. The threshold voltage and series resistance of the p–n diode are 3 V and 3.8×10^4 Ω, respectively. The higher threshold voltage of the SIS diode is attributed to impact ionization at a high voltage, which occurred because of carriers tunneling through the insulating layer.[19,41] The relatively higher series resistance compared with a conventional Si-based diode is mainly attributed to the lower sheet resistance of p-GaN. The currents at 20 V for the SIS and p–n diode structures are 2.2×10^{-3} and 4.5×10^{-4} A, respectively. The current of the SIS heterojunction diode, which is approximately 5 times higher than that of the p–n heterojunction diode, supports the fact that a relatively large number of carriers flow through the SIS heterojunction diode *via* tunneling, as compared with the conventional carrier transport in the p–n heterojunction. Moreover, the current of the SIS diode is approximately 10^5 times higher than that in the previously reported van der Waals heterojunction device, although the threshold voltage of the SIS diode is higher.[17,42] To confirm the leakage current of the SIS and p–n diode structures, *I*–*V* measurements of p-GaN were carried out. As a result, a significantly higher leakage current and linear *I*–*V* curve were observed in p-GaN, as shown in the Supporting Information (Figure S2). Note that the very weak current-rectifying characteristics of the p–n heterojunction are attributed to the extremely thin 1-L MoS_2 layer, which could be entirely depleted.

The carrier transport mechanisms for both samples at equilibrium and under forward and reverse biases are illustrated in Figure 4. The work functions of p-GaN and 1-L MoS_2 are ~7.5 and 4.6–4.9 eV, respectively.[43,44] The built-in potential of the p–n junction is approximately 3 eV. The electron affinities of p-GaN and MoS_2 are 4.1 and 4.2 eV, respectively.[44,45] As the last parameters for the energy band diagram, the direct optical transition band of p-GaN and 1-L MoS_2 are 3.4 and 1.8 eV, respectively.[44,46] On the basis of these parameters, the energy band diagram of the p–n heterojunction structure is expected to consist of p-GaN and 1-L MoS_2, as depicted in Figure 4a, under zero bias. The built-in potential of the p–n heterojunction structure should decrease as a function of the forward bias. Above the threshold voltage, the current flow could dramatically increase due to carrier transport, as depicted in Figure 4b. On the contrary, carriers cannot flow under a reverse bias because of a large built-in potential, as shown in Figure 4c. This carrier transport scheme matches the experimental results of the *I*–*V* curve well, as shown in Figure 3b. For the SIS heterojunction structure, the electron affinity and energy band gap of h-BN are 2–2.3 and 5.2–5.9 eV, respectively.[44] The energy band diagram of the SIS heterojunction structure consisting of p-GaN, h-BN, and 1-L MoS_2 at equilibrium is illustrated in Figure 4d using the energy band parameters. When the forward bias increases, carriers can be accumulated at the interface between the semiconductor and the

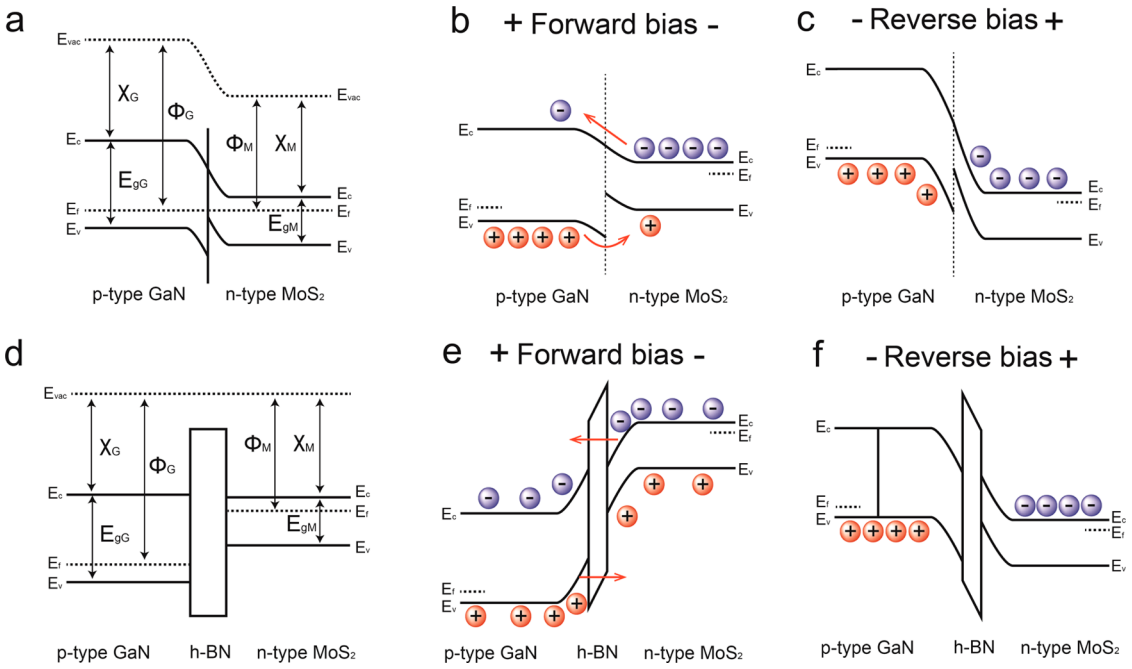

Figure 4. Energy band diagrams of p−n heterojunction structures under (a) zero bias, (b) forward bias, and (c) reverse bias. Carrier transport can be explained by referring to the conventional p−n heterojunction characteristics. Energy band diagrams of the SIS heterojunction structure under (d) zero bias, (e) forward bias, and (f) reverse bias. Tunneling was the predominant carrier transport mechanism for the SIS structure.

insulator. The accumulated carriers abruptly flow above the threshold voltage, with a large number of carriers tunneling through the insulating layer, as shown in Figure 4e. On the other hand, current cannot flow under a reverse bias due to the high potential barrier, as depicted in Figure 4f. This tunneling mechanism can explain the current-rectifying behavior at a high current, as shown in Figure 3a. By examining the *I*−*V* curves and carrier transport mechanisms for both samples, we can conclude that the SIS heterojunction structure has a much higher current flow compared with that of the p−n heterojunction structure because of carrier tunneling.

To investigate the photoresponse of the SIS heterojunction diode, photocurrent measurements were carried out by using a conventional *I*−*V* probe station with a visible-light source with a spectral range from approximately 400 to 700 nm, as shown in Figure S3 of the Supporting Information. The size of the light spot was approximately 7 cm, and it had a circular shape. A constant voltage of 9 V was applied to the SIS heterojunction diode to measure the time-dependent photocurrent, as shown in Figure 5. The current increased when the light source was turned on, and the photocurrent rapidly decayed when the light source was turned off. The rise and decay times of the photocurrent were 0.5 and 0.3 s, respectively. These rise and decay times are much shorter than the previously reported times of 4 and 9 s, respectively.[11] The I_{light}/I_{dark} ratio was as high as approximately 560 at an incident light intensity of 8 mW, and a photoresponsivity of

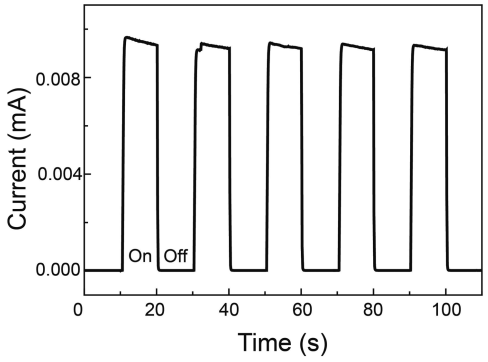

Figure 5. Photocurrent of the SIS structure induced by illumination *via* visible light. The photocurrent decayed when the light source was switched off.

1.2 mA/W was calculated. This indicates that the SIS heterojunction structure can be applied to optoelectronic devices such as photodiodes and solar cells because the photoresponsivity of the SIS heterojunction structure is highly sensitive to visible light.

CONCLUSIONS

We have presented a SIS heterojunction diode that consists of 1-L MoS_2, h-BN, and p-GaN as the top semiconductor, insulator, and bottom semiconductor, respectively. The layered materials of 1-L MoS_2 and h-BN are vertically stacked by a chemical transfer method on the p-GaN substrate, which itself was grown by metal−organic chemical vapor deposition. The crystalline qualities of each layer and the final stacked structure were confirmed by confocal photoluminescence and Raman

spectroscopy. From the $I-V$ measurements, the device exhibits a clear current-rectifying characteristic, which was observed in both the p−n and SIS heterojunction structures. However, a higher current and threshold voltage were observed for the SIS structure compared with the p−n structure. The increase in the current and the higher threshold voltage indicate that the predominant carrier transport mechanism is tunneling. Moreover, a sensitive photoresponse was observed for the SIS structure by photocurrent measurements. This SIS heterojunction structure consisting of layered 1-L MoS_2, h-BN, and epitaxial p-GaN is expected to be a promising device for nanoscale electronics, optoelectronics, and integrated circuits.

EXPERIMENTAL METHODS

Fabrication of p-Type GaN. p-GaN was grown by metal−organic chemical vapor deposition. Trimethylgallium and ammonia were employed as precursors for Ga and N, respectively. N_2 gas was used as the carrier gas. Following epitaxial growth, a thermal annealing process was carried out at 940 °C for 40 s to activate the hole carriers.

Fabrication of h-BN. h-BN was grown by CVD on a metal foil with borazine as the precursor. For the transfer of h-BN, poly(methyl methacrylate) (PMMA) was used as the supporting material. The grown h-BN layer was coated with PMMA, and the metal foil was etched by a chemical etchant. Then, the residual chemical etchant on the backside of the h-BN was removed by a diluted HCl solution. The h-BN with PMMA was transferred to p-type GaN. Acetone was used to remove the PMMA on the transferred h-BN. Finally, the h-BN was annealed at 500 °C for 3 h to improve its crystalline quality.

Fabrication of Monolayer MoS_2. Monolayer MoS_2 was grown by the CVD method on a SiO_2 substrate. As a supporting material, the grown 1-L MoS_2 was coated with PMMA during the chemical etching of SiO_2. A diluted HF solution was used to etch the SiO_2 layer. The 1-L MoS_2 with PMMA was separated from the SiO_2 substrate and transferred onto a prepared template consisting of p-type GaN and h-BN. The template was dried at 80 °C for 1 h to remove residual water.

Characterization of the SIS Diode. Confocal photoluminescence spectroscopy, including a high numerical aperture (0.7) objective lens, was used to measure the PL spectra. The excitation sources were 355 and 532 nm diode-pumped solid-state lasers for p-type GaN and 1-L MoS_2, respectively. Confocal Raman mapping was conducted by commercial multifunctional microscopy (NTEGRA, NT-MDT) with a pinhole size of 50 μm. To disperse the light collected from the samples, a 30 cm monochromator (SP2300, Princeton Instruments) was employed. For detection of the optical signal, a thermoelectrically cooled charge-coupled device was used (PIXIS100, Princeton Instruments). A conventional probe station system equipped with a power supply and source measurement unit (Keithley 2400) was used for the $I-V$ curves.

Conflict of Interest: The authors declare no competing financial interest.

Acknowledgment. This work was supported by IBS-R011-D1 of Korea and the Human Resources Development program (No. 20124010203270) of the Korea Institute of Energy Technology Evaluation and Planning (KETEP), funded by the Ministry of Trade, Industry and Energy of the Korean government, and partially supported by the FUI MULTISS project (F1305008 M). K.K.K. acknowledges the support from Basic Science Research Program through the National Research Foundation of Korea (NRF) funded by the Ministry of Science, ICT & Future Planning (2015R1C1A1A02037083).

Supporting Information Available: The Supporting Information is available free of charge on the ACS Publications website at DOI: 10.1021/acsnano.5b04233.

Confocal Raman spectroscopy of p-GaN, $I-V$ curve of p-GaN layer, and the light emission spectrum in the visible light for photocurrent (PDF)

REFERENCES AND NOTES

1. Bonaccorso, F.; Colombo, L.; Yu, G.; Stoller, M.; Tozzini, V.; Ferrari, A. C.; Ruoff, R. S.; Pellegrini, V. Graphene, Related Two-Dimensional Crystals, and Hybrid Systems for Energy Conversion and Storage. *Science* **2015**, *347*, 6217.
2. Chen, Z.; Ren, W.; Gao, L.; Liu, B.; Pei, S.; Cheng, H.-M. Three-Dimensional Flexible and Conductive Interconnected Graphene Networks Grown by Chemical Vapour Deposition. *Nat. Mater.* **2011**, *10*, 424–428.
3. Addou, R.; Dahal, A.; Batzill, M. Growth of A Two-Dimensional Dielectric Monolayer on Quasi-Freestanding Graphene. *Nat. Nanotechnol.* **2013**, *8*, 41–45.
4. Woessner, A.; Lundeberg, M. B.; Gao, Y.; Principi, A.; Alonso-González, P.; Carrega, M.; Watanabe, K.; Taniguchi, T.; Vignale, G.; Polini, M.; et al. Highly Confined Low-Loss Plasmons in Graphene−Boron Nitride Heterostructures. *Nat. Mater.* **2015**, *14*, 421–425.
5. Withers, F.; Del Pozo-Zamudio, O.; Mishchenko, A.; Rooney, A. P.; Gholinia, A.; Watanabe, K.; Taniguchi, T.; Haigh, S. J.; Geim, A. K.; Tartakovskii, A. I.; et al. Light-Emitting Diodes by Band-Structure Engineering in Van Der Waals Heterostructures. *Nat. Mater.* **2015**, *14*, 301–306.
6. Wang, Q. H.; Kalantar-Zadeh, K.; Kis, A.; Coleman, J. N.; Strano, M. S. Electronics and Optoelectronics of Two-Dimensional Transition Metal Dichalcogenides. *Nat. Nanotechnol.* **2012**, *7*, 699–712.
7. Lee, K.; Gatensby, R.; McEvoy, N.; Hallam, T.; Duesberg, G. S. High-Performance Sensors Based on Molybdenum Disulfide Thin Films. *Adv. Mater.* **2013**, *25*, 6699–6702.
8. Radisavljevic, B.; Kis, A. Mobility Engineering and A Metal−Insulator Transition in Monolayer MoS_2. *Nat. Mater.* **2013**, *12*, 815–820.
9. Splendiani, A.; Sun, L.; Zhang, Y.; Li, T.; Kim, J.; Chim, C.-Y.; Galli, G.; Wang, F. Emerging Photoluminescence in Monolayer MoS_2. *Nano Lett.* **2010**, *10*, 1271–1275.
10. Radisavljevic, B.; Radenovic, A.; Brivio, J.; Giacometti, V.; Kis, A. Single-Layer MoS_2 Transistors. *Nat. Nanotechnol.* **2011**, *6*, 147–150.
11. Lopez-Sanchez, O.; Lembke, D.; Kayci, M.; Radenovic, A.; Kis, A. Ultrasensitive Photodetectors Based on Monolayer MoS_2. *Nat. Nanotechnol.* **2013**, *8*, 497–501.
12. Schmidt, H.; Wang, S.; Chu, L.; Toh, M.; Kumar, R.; Zhao, W.; Castro Neto, A. H.; Martin, J.; Adam, S.; Özyilmaz, B.; et al. Transport Properties of Monolayer MoS_2 Grown by Chemical Vapor Deposition. *Nano Lett.* **2014**, *14*, 1909–1913.
13. Bernardi, M.; Palummo, M.; Grossman, J. C. Extraordinary Sunlight Absorption and One Nanometer Thick Photovoltaics Using Two-Dimensional Monolayer Materials. *Nano Lett.* **2013**, *13*, 3664–3670.
14. Terrones, H.; López-Urías, F.; Terrones, M. Novel Hetero-Layered Materials with Tunable Direct Band Gaps by Sandwiching Different Metal Disulfides and Diselenides. *Sci. Rep.* **2013**, *3*, 1549.
15. Dai, J.; Zeng, X. C. Bilayer phosphorene: Effect of Stacking Order on Bandgap and Its Potential Applications in Thin-Film Solar Cells. *J. Phys. Chem. Lett.* **2014**, *5*, 1289–1293.
16. Geim, A. K.; Grigorieva, I. V. Van Der Waals Heterostructures. *Nature* **2013**, *499*, 419–425.
17. Lee, C.-H.; Lee, G.-H.; van der Zande, A. M.; Chen, W.; Li, Y.; Han, M.; Cui, X.; Arefe, G.; Nuckolls, C.; Heinz, T. F.; et al. Atomically Thin P−N Junctions with Van Der Waals Heterointerfaces. *Nat. Nanotechnol.* **2014**, *9*, 676–681.
18. Gong, Y.; Lin, J.; Wang, X.; Shi, G.; Lei, S.; Lin, Z.; Zou, X.; Ye, G.; Vajtai, R.; Yakobson, B. I.; et al. Vertical and In-Plane

Heterostructures From WS_2/MoS_2 Monolayers. *Nat. Mater.* **2014**, *13*, 1135–1142.
19. Shewchun, J.; Temple, V. A. K. Theoretical Tunneling Current Characteristics of The SIS (semiconductor-insulator-semiconductor) Diode. *J. Appl. Phys.* **1972**, *43*, 5051–5061.
20. Shewchun, J.; Dubow, J.; Myszkowski, A.; Singh, R. The Operation of The Semiconductor-Insulator-Semiconductor (SIS) Solar Cell: Theory. *J. Appl. Phys.* **1978**, *49*, 855–864.
21. Shewchun, J.; Dubow, J.; Wilmsen, C. W.; Singh, R.; Burk, D.; Wager, J. F. The Operation of The Semiconductor-Insulator-Semiconductor Solar Cell: Experiment. *J. Appl. Phys.* **1979**, *50*, 2832–2839.
22. Bykhovski, A.; Gelmont, B.; Shur, M. Strain and Charge Distribution in GaN-AlN-GaN Semiconductor-Insulator-Semiconductor Structure for Arbitrary Growth Orientation. *Appl. Phys. Lett.* **1993**, *63*, 2243–2245.
23. Arnold, D.; Ketterson, A.; Henderson, T.; Klem, J.; Morkoç, H. Electrical Characterization of GaAs/AlGaAs Semiconductor-Insulator-Semiconductor Capacitors and Application to The Measurement of The GaAs/AlGaAs Band-Gap Discontinuity. *J. Appl. Phys.* **1985**, *57*, 2880–2885.
24. Tonndorf, P.; Schmidt, R.; Böttger, P.; Zhang, X.; Börner, J.; Liebig, A.; Albrecht, M.; Kloc, C.; Gordan, O.; Zahn, D. R. T.; et al. Photoluminescence Emission and Raman Response of Monolayer MoS_2, $MoSe_2$, and WSe_2. *Opt. Express* **2013**, *21*, 4908–4916.
25. Mouri, S.; Miyauchi, Y.; Matsuda, K. Tunable Photoluminescence of Monolayer MoS_2 *via* Chemical Doping. *Nano Lett.* **2013**, *13*, 5944–5948.
26. Islam, M. R.; Kang, N.; Bhanu, U.; Paudel, H. P.; Erementchouk, M.; Tetard, L.; Leuenberger, M. N.; Khondaker, S. I. Tuning The Electrical Property *via* Defect Engineering of Single Layer MoS_2 by Oxygen Plasma. *Nanoscale* **2014**, *6*, 10033–10039.
27. Chichibu, S.; Azuhata, T.; Sota, T.; Nakamura, S. Excitonic Emissions From Hexagonal GaN Epitaxial Layers. *J. Appl. Phys.* **1996**, *79*, 2784–2786.
28. Katz, O.; Bahir, G.; Salzman, J. Persistent Photocurrent and Surface Trapping in GaN Schottky Ultraviolet Detectors. *Appl. Phys. Lett.* **2004**, *84*, 4092–4094.
29. Jeong, H.; Jeong, S. Y.; Park, D. J.; Jeong, H. J.; Jeong, S.; Han, J. T.; Jeong, H. J.; Yang, S.; Kim, H. Y.; Baeg, K.-J.; et al. Suppressing Spontaneous Polarization of P-GaN by Graphene Oxide Passivation: Augmented Light Output of GaN UV-LED. *Sci. Rep.* **2015**, *5*, 7778.
30. Jeong, H.; Jeong, H. J.; Oh, H. M.; Hong, C.-H.; Suh, E.-K.; Lerondel, G.; Jeong, M. S. Carrier Localization in In-Rich InGaN/GaN Multiple Quantum Wells for Green Light-Emitting Diodes. *Sci. Rep.* **2015**, *5*, 9373.
31. Jeong, H.; Park, D. J.; Lee, H. S.; Ko, Y. H.; Yu, J. S.; Choi, S.-B.; Lee, D.-S.; Suh, E.-K.; Jeong, M. S. Light-Extraction Enhancement of A GaN-Based LED Covered With ZnO Nanorod Arrays. *Nanoscale* **2014**, *6*, 4371–4378.
32. Chang, C.-W.; Tan, W.-C.; Lu, M.-L.; Pan, T.-C.; Yang, Y.-J.; Chen, Y.-F. Graphene/SiO_2/p-GaN Diodes: An Advanced Economical Alternative for Electrically Tunable Light Emitters. *Adv. Funct. Mater.* **2013**, *23*, 4043–4048.
33. Liao, J.; Sa, B.; Zhou, J.; Ahuja, R.; Sun, Z. Design of High-Efficiency Visible-Light Photocatalysts for Water Splitting: MoS_2/AlN(GaN) Heterostructures. *J. Phys. Chem. C* **2014**, *118*, 17594–17599.
34. Wang, L.; Wu, B.; Chen, J.; Liu, H.; Hu, P.; Liu, Y. Monolayer Hexagonal Boron Nitride Films With Large Domain Size and Clean Interface for Enhancing The Mobility of Graphene-Based Field-Effect Transistors. *Adv. Mater.* **2014**, *26*, 1559–1564.
35. Kim, K. K.; Hsu, A.; Jia, X.; Kim, S. M.; Shi, Y.; Dresselhaus, M.; Palacios, T.; Kong, J. Synthesis and Characterization of Hexagonal Boron Nitride Film as A Dielectric Layer for Graphene Devices. *ACS Nano* **2012**, *6*, 8583–8590.
36. Chung, S. J.; Suh, E. K.; Lee, H. J.; Mao, H. B.; Park, S. J. Photoluminescence and Photocurrent Studies of P-type GaN With Various Thermal Treatments. *J. Cryst. Growth* **2002**, *235*, 49–54.
37. Eda, G.; Yamaguchi, H.; Voiry, D.; Fujita, T.; Chen, M.; Chhowalla, M. Photoluminescence From Chemically Exfoliated MoS_2. *Nano Lett.* **2011**, *11*, 5111–5116.
38. Mak, K. F.; He, K.; Lee, C.; Lee, G. H.; Hone, J.; Heinz, T. F.; Shan, J. Tightly Bound Trions in Monolayer MoS_2. *Nat. Mater.* **2013**, *12*, 207–211.
39. Docherty, C. J.; Parkinson, P.; Joyce, H. J.; Chiu, M.-H.; Chen, C.-H.; Lee, M.-Y.; Li, L.-J.; Herz, L. M.; Johnston, M. B. Ultrafast Transient Terahertz Conductivity of Monolayer MoS_2 and WSe_2 Grown by Chemical Vapor Deposition. *ACS Nano* **2014**, *8*, 11147–11153.
40. Feigelson, B. N.; Bermudez, V. M.; Hite, J. K.; Robinson, Z. R.; Wheeler, V. D.; Sridhara, K.; Hernandez, S. C. Growth and Spectroscopic Characterization of Monolayer and Few-Layer Hexagonal Boron Nitride on Metal Substrates. *Nanoscale* **2015**, *7*, 3694–3702.
41. Hwang, D.-K.; Oh, M.-S.; Lim, J.-H.; Choi, Y.-S.; Park, S.-J. ZnO-Based Light-Emitting Metal-Insulator-Semiconductor Diodes. *Appl. Phys. Lett.* **2007**, *91*, 121113.
42. Furchi, M. M.; Pospischil, A.; Libisch, F.; Burgdörfer, J.; Mueller, T. Photovoltaic Effect in An Electrically Tunable Van Der Waals Heterojunction. *Nano Lett.* **2014**, *14*, 4785–4791.
43. Kim, H.-K.; Adesida, I.; Seong, T.-Y. Interfacial Reaction Effect on The Ohmic Properties of A Pt/Pd/Au Contact on P-type GaN. *J. Vac. Sci. Technol., A* **2004**, *22*, 1101–1104.
44. Sup Choi, M.; Lee, G.-H.; Yu, Y.-J.; Lee, D.-Y.; Hwan Lee, S.; Kim, P.; Hone, J.; Jong Yoo, W. Controlled Charge Trapping by Molybdenum Disulphide and Graphene in Ultrathin Heterostructured Memory Devices. *Nat. Commun.* **2013**, *4*, 1624.
45. Wang, L.; Nathan, M. I.; Lim, T. H.; Khan, M. A.; Chen, Q. High Barrier Height GaN Schottky Diodes: Pt/GaN and Pd/GaN. *Appl. Phys. Lett.* **1996**, *68*, 1267–1269.
46. Muth, J. F.; Lee, J. H.; Shmagin, I. K.; Kolbas, R. M.; Casey, H. C.; Keller, B. P.; Mishra, U. K.; DenBaars, S. P. Absorption Coefficient, Energy Gap, Exciton Binding Energy, and Recombination Lifetime of GaN Obtained From Transmission Measurements. *Appl. Phys. Lett.* **1997**, *71*, 2572–2574.